Asymmetric Collaborative Bar Stabilization Tethered to Two Heterogeneous Aerial Vehicles

Pedro O. Pereira, Pedro Roque and Dimos V. Dimarogonas

***Abstract*— We consider a system composed of a bar tethered to two unmanned aerial vehicles (UAVs), where the cables behave as rigid links under tensile forces, and with the control objective of stabilizing the bar's pose around a desired pose. Each UAV is equipped with a PID control law, and we verify that the bar's motion is decomposable into three decoupled motions, namely a longitudinal, a lateral and a vertical. We then provide relations between the UAVs' gains, which, if satisfied, allows us to decompose each of those motions into two cascaded motions; the latter relations between the UAVs' gains are found so as to counteract the system asymmetries, such as the different cable lengths and the different UAVs' weights. Finally, we provide conditions, based on the system's physical parameters, that describe *good* and *bad* types of asymmetries. We present experiments that demonstrate the stabilization of the bar's pose.**

I. Introduction

Aerial vehicles provide a platform for transportation of cargos in dangerous and cluttered environments [1]. In particular, vertical take off and landing rotorcrafts, with hovering capabilities, have been used to validate different types of transportation and manipulation of objects.

Tethered transportation, when compared with manipulator-endowed transportation, is mechanically simple and inexpensive. Several control strategies for slung-load transportation, i.e., tethered transportation of a point mass load by a single UAV, are found in the literature. The swing angle of the load can be estimated, either inferred from vision or from the internal force exerted by the load on the UAV, and used in the feedback loop to avoid/dampen swing excitation [2], [3]. Trajectory planning that minimizes the loads' swing, and exploiting differential flatness for control purposes has also been demonstrated [4]–[6].

Cooperative transportation with multiple UAVs is also found in the literature. Vision has been used to correctly place end-effectors with respect to a visual target placed on the object to be transported [7], [8], or to autonomously estimate the bar's pose [9]. Motion planning for collision avoidance between the cargo and the UAVs with obstacles in a cluttered environment has also been studied and validated [10]–[12]. How to position a group of UAVs by specifying the desired tension on the cables and a desired pose for the tethered object is found in [13], [14]. Note that tethered transportation with multiple UAVs comes with multiple degrees of freedom, which have been explored so as to minimize the internal forces applied of the load [15], [16]. There are different grasping mechanisms in aerial transportation, such as, adhesive/gripping mechanisms at the tool-tip that stick to the grasped object [17]; a hook-based system between the end-effector and the point to grasp [12]; and magnets, electromagnets and electropermanent magnets [18] – the latter is the option we adopt.

The authors are with the School of Electrical Engineering, KTH Royal Institute of Technology, SE-100 44, Stockholm, Sweden. {ppereira, dimos}@kth.se. This work was supported by the EU H2020 Research and Innovation Programme under GA No.644128 (AEROWORKS), the Swedish Research Council (VR), the Swedish Foundation for Strategic Research (SSF) and the KAW Foundation.

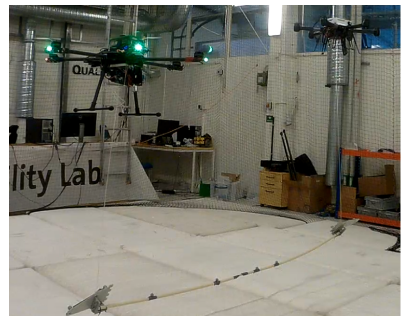

Fig. 1: Tethered transportation of a rod-like object by two heterogeneous aerial vehicles, with different cable lengths.

In this manuscript, we focus on stabilization of a rod-like object tethered to two AUVs, as pictured in Fig. 1. This problem has also been considered in [9], [19], [20]. In [19], a master-slave approach for the two UAVs is put in place, with the slave UAV estimating the cable force exerted on itself. In [9], vision is used to autonomously estimate the bar's pose. In [20], relations on the UAVs' PID gains are provided for which stability – regarding the bar's pose stabilization – is guaranteed.

Regarding experimental cooperative transportation, experiments have been performed where the system is taken to be symmetric [9], [9], [12], [19], [20]. In this work, we extend [20], and consider an asymmetric system, with non-identical UAVs and different cable lengths. We perform an analysis similar to that in [21]–[23], where we linearize the system, and derive conditions on the gains that guarantee exponential stability regarding the stabilization of the bar's pose. We verify that the bar's motion is decomposable into three decoupled motions, namely a longitudinal, a lateral and a vertical; and that if UAVs' gains satisfy specific relations, each of those motions is in turn decomposable into two cascaded motions: e.g., the vertical motion is decomposable into the vertical linear motion and the vertical angular motion of the bar, with the latter cascaded after the former, if the vertical PID gains of the two UAVs satisfy a specific ratio. Finally, we provide conditions, based on the system's physical parameters, that describe *good* and *bad* types of asymmetries, which may be explored to design safer experiments.

The remainder of this paper is structured as follows. In

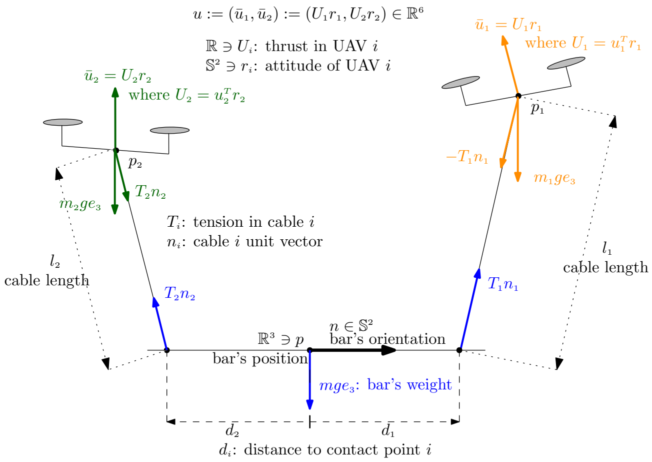

Fig. 2: Modeling of the UAVs-bar system

Sections III and IV, the model of the system and the contol law are described. In Section V, we present conditions under which matrices of interest are Hurwitz. In Section VI, we linearize the closed loop vector field around the equilibrium and, under a proper similarity transformation and a proper choice of gains, we verify the longitudinal, lateral and vertical motion decomposition. Finally, in Section VII, we present illustrative experimental results.

II. Notation

The map $\mathcal{S} : \mathbb{R}^3 \ni x \mapsto \mathcal{S}(x) \in \mathbb{R}^{3\times 3}$ yields a skew-symmetric matrix and it satisfies $\mathcal{S}(a)\, b = a \times b$, for any $a, b \in \mathbb{R}^3$. $\mathbb{S}^2 := \{x \in \mathbb{R}^3 : x^T x = 1\}$ denotes the set of unit vectors in $\mathbb{R}^3$. We denote $A_1 \oplus \cdots \oplus A_n$ as the block diagonal matrix with block diagonal entries A_1 to A_n (square matrices). We denote by $e_1, \cdots, e_n \in \mathbb{R}^n$ the canonical basis vectors in $\mathbb{R}^n$, for some $n \in \mathbb{N}$. Given some $n, m \in \mathbb{N}$, and a function $f : \mathbb{R}^n \ni a \mapsto f(a) \in \mathbb{R}^m$, $f' : \mathbb{R}^n \ni a \mapsto f'(a) \in \mathbb{R}^{m\times n}$ denotes the derivative of f.

III. Problem Description

Consider the system illustrated in Fig. 2, with two VTOL aerial vehicles, a one dimensional bar and two cables connecting the aerial vehicles to distinct contact points on the bar. Fig. 2 provides a two-dimensional picture of the real system, as shown in Fig 1, but the modeling we describe next is three dimensional. Hereafter, and for brevity, we refer to this system as UAVs-bar system. We denote by $p_1, p_2, p \in \mathbb{R}^3$ and by $v_1, v_2, v \in \mathbb{R}^3$ the UAVs' and the bar's center of mass positions and velocities; by $n, \omega \in \mathbb{R}^3$ the bar's orientation and angular velocity; by $r_1, r_2 \in \mathbb{S}^2$ the UAVs' thrust body directions; and by $\xi_1, \xi_2 \in \mathbb{R}$ the vertical integral error of each UAV. As for physical constants, we denote by $m_1, m_2, m > 0$ the UAVs' and bar's masses; by $J > 0$ the bar's moment of inertia (w.r.t. the bar's center of mass); by $l_1, l_2 > 0$ the cables' lengths; and, finally, by $d_1, d_2 \in \mathbb{R}$ the contact points on the bar at which the cables are attached to. Finally, we denote by $u_1, u_2 \in \mathbb{R}^3$ the input forces on the UAVs-bar system: for $i \in \{1, 2\}$, $\bar{u}_i := U_i r_i := u_i^T r_i r_i$ is the UAV i input force, where the throttle U_i is taken as the inner product between the input u_i and the UAV's thrust body direction (one may think of u_i as the desired value for $\bar{u}_i$).

For brevity, given the quantities described above, denote

$$
\begin{aligned}
z &:= (p, n, p_1, p_2, v, \omega, v_1, v_2, r_1, r_2, \xi_1, \xi_2) \in \mathbb{R}^{32}, \\
u &:= (u_1, u_2) \in \mathbb{R}^6,
\end{aligned}
\tag{1}
$$

where z and u are used next as the state and input, respectively, of the UAVs-bar system. Consider then the state space

$$
\mathbb{Z} := \{z \in \mathbb{R}^{32} : f(z) = 0_8\}, \tag{2}
$$

$$
f(z) := \begin{bmatrix} n^T n - 1 \\ n^T \omega \\ \|p + d_1 n - p_1\|^2 - l_1^2 \\ \|p + d_2 n - p_2\|^2 - l_2^2 \\ (p + d_1 n - p_1)^T (v + d_1 \mathcal{S}(\omega)\, n - v_1) \\ (p + d_2 n - p_2)^T (v + d_2 \mathcal{S}(\omega)\, n - v_2) \\ r_1^T r_1 - 1 \\ r_2^T r_2 - 1 \end{bmatrix}, \tag{3}
$$

where the map f defined above encapsulates the constraints illustrated in Fig. 2. Specifically, the first two constraints in (3) imply that the bar's attitude n is given by a unit vector and that the bar's angular velocity ω is orthogonal to that unit vector; the next four constraints in (3), imply that the distance between each contact point on the bar and the corresponding UAV is constant and equal to the corresponding cable length; and, finally, the last two constraints in (3), imply that the UAVs' thrust vectors are also given by unit vectors.

Given an appropriate input $u : \mathbb{R}_{\geq 0} \to \mathbb{R}^6$, a system's trajectory $z : \mathbb{R}_{\geq 0} \ni t \mapsto z(t) \in \mathbb{Z}$ evolves according to

$$
\dot{z}(t) = Z(z(t), u(t)), z(0) \in \mathbb{Z}, \tag{4}
$$

where the vector field $Z : \mathbb{Z} \times \mathbb{R}^6 \ni (z, u) \mapsto Z(z, u) \in \mathbb{R}^{32}$ is given by

$$
Z(z, u) := \begin{bmatrix} Z_k(z) \\ Z_d(z, u) \\ Z_r(z, u) \\ Z_i(z) \end{bmatrix} \left(= \begin{bmatrix} \text{kinematics} \\ \text{dynamics} \\ \text{attitude inner loop} \\ \text{integrator dynamics} \end{bmatrix} \right), \tag{5}
$$

with the kinematics given by

$$
Z_k(z) := (v, \mathcal{S}(\omega)\, n, v_1, v_2) \left(= (\dot{p}, \dot{n}, \dot{p}_1, \dot{p}_2)\right),
$$

with the dynamics given by (below, g stands for the acceleration due to gravity; T_1, T_2 stand for the tensions on the cables, which are functions of the state and the input; and $n_i \equiv \frac{p_i - (p + d_i n)}{l_i}$ stands for the cable $i \in \{1, 2\}$ direction)

$$
Z_d(z, u) := \begin{bmatrix} \sum_{i\in\{1,2\}} \frac{T_i(z,\bar{u})}{m} n_i - g e_3 \\ \sum_{i\in\{1,2\}} \frac{T_i(z,\bar{u})}{J} \mathcal{S}(d_i n)\, n_i \\ \frac{\bar{u}_1}{m_1} - \frac{T_1(z,\bar{u})}{m_1} n_1 - g e_3 \\ \frac{\bar{u}_2}{m_2} - \frac{T_2(z,\bar{u})}{m_2} n_2 - g e_3 \end{bmatrix} \left(= \begin{bmatrix} \dot{v} \\ \dot{\omega} \\ \dot{v}_1 \\ \dot{v}_2 \end{bmatrix} \right),
$$

$$
\bar{u} \equiv (\bar{u}_1, \bar{u}_2) \equiv (u_1^T r_1 r_1, u_2^T r_2 r_2),
$$

with the attitude inner loop dynamics given by (below, k_r^1, k_r^2 stand for the positive gains of the UAVs' attitude inner loop)

$$
Z_r(z, u) := \begin{bmatrix} \mathcal{S}\left(k_r^1 \mathcal{S}(r_1) \frac{u_1}{\|u_1\|}\right) r_1 \\ \mathcal{S}\left(k_r^2 \mathcal{S}(r_2) \frac{u_2}{\|u_2\|}\right) r_2 \end{bmatrix} \left(= \begin{bmatrix} \dot{r}_1 \\ \dot{r}_2 \end{bmatrix} \right), \tag{6}
$$

and, finally, with the integrator dynamics given by

$$Z_i(z,u) := \begin{bmatrix} e_3^T p_1 - l_1 \\ e_3^T p_2 - l_2 \end{bmatrix} \left(= \begin{bmatrix} \dot{\xi}_1 \\ \dot{\xi}_2 \end{bmatrix} \right). \tag{7}$$

An important relation to note is that

$$\underbrace{f'(z)}_{\mathbb{R}^{8\times 32}} \underbrace{Z(z,u)}_{\mathbb{R}^{32}} = 0_8, \text{ for all } (z,u) \in \mathbb{Z} \times \mathbb{R}^6, \tag{8}$$

which implies that a solution of (4) starting in $\mathbb{Z}$, remains in $\mathbb{Z}$ (i.e., that $\mathbb{Z}$ is invariant).

Let us provide some details on the vector field (5). The dynamics equations are obtained from the Newton-Euler's equations of motion, considering the net force and torque on each rigid body: the bar is taken as a rigid body (with net force and torque in blue – see Fig. 2); while the UAVs are taken as point masses (with net forces in orange and green – see Fig. 2). The Newton-Euler's equations of motion do not provide any insight into the tensions T_1 and T_2 since these constitute internal forces: the tensions are found by requiring the dynamics to belong to the state space tangent set. The explicit description on the tensions is found in [24], but it is omitted here for brevity. The attitude inner loop dynamics in (6) corresponds to a first order model with attitude gain $k_r^i > 0$, that guarantees that the UAV $i \in \{1,2\}$ thrust vector tries to align itself with the direction of the input force u_i (for a constant $u_i \in \mathbb{R}^3 \backslash \{0_3\}$, a solution of $\dot{r}_i = -k_r \mathcal{S}(r_i) \mathcal{S}(r_i) \frac{u_i}{\|u_i\|}$ converges exponentially fast to $\frac{u_i}{\|u_i\|}$, with rate proportional to k_r). Note that the model for the UAVs' attitude inner loop in (6) is only a possible one, and there are more ways of modeling that inner loop.

Let us define the equilibrium, before explaining the integrator dynamics in (7). For any $(\xi_1^\star, \xi_2^\star) \in \mathbb{R}^2$, define

$$\begin{aligned} z^\star &:= (p^\star, n^\star, p_1^\star, p_2^\star, v^\star, \omega^\star, v_1^\star, v_2^\star, r_1^\star, r_2^\star, \xi_1^\star, \xi_2^\star) \in \mathbb{Z} \\ &:= (0_3, e_1, d_1 e_1 + l_1 e_3, d_2 e_1 + l_2 e_3, 0_3, 0_3, 0_3, 0_3, e_3, e_3, \xi_1^\star, \xi_2^\star), \end{aligned} \tag{9}$$

and $u^\star := (u_1^\star, u_2^\star) \in \mathbb{R}^6$ as

$$u^\star := \left(\left(m_1 + \frac{m d_2}{d_2 - d_1} \right) g e_3, \left(m_2 + \frac{m d_1}{d_1 - d_2} \right) g e_3 \right). \tag{10}$$

Since it can be verified that $Z(z^\star, u^\star) = 0_{32}$, it follows that $z^\star$ (under a constant input $u^\star$) is an equilibrium of the system. Thus, the integral terms (ξ_1, ξ_2) evolving according to the integrator dynamics in (7) represent the vertical-position integral error of the UAVs. These integral errors are used in the control law, and provide robustness again disturbances and model uncertainties, as shall be verified in the experiments.

We can now formulate the problem treated in this paper.

Problem 1: Given the vector field Z in (5) and the equilibrium $z^\star$ in (9) (for some $(\xi_1^\star, \xi_2^\star) \in \mathbb{R}^2$), design a control law $u^{cl} : \mathbb{Z} \to \mathbb{R}^6$ satisfying $u^{cl}(z^\star) = u^\star$ and such that $z^\star$ is an exponentially stable equilibrium of the closed loop vector field $z \mapsto Z(z, u^{cl}(z))$.

Remark 1: In general, we may require the bar to stabilize around any point $p^\star \in \mathbb{R}^3$ and any attitude $n^\star \in \mathbb{S}^2$ with $e_3^T n^\star = 0$. For that purpose, if suffices to place the origin of the inertial frame at $p^\star$, and align the inertial x-axis with $n^\star$: i.e., stabilizing around the pose $(p^\star, n^\star)$ is reduced to stabilizing around the pose $(0_3, e_1)$ as indicated in the equilibrium (9).

Definition 1: We say the system is symmetric if

$$m_1 = m_2 =: M, l_1 = l_2 =: l, \text{ and } d_1 = -d_2 =: d. \tag{11}$$

IV. Control Law

For each aerial vehicle – $j \in \{1,2\}$ – consider the PID-like control law $u_j^{pid} : \mathbb{Z} \ni z \mapsto u_j^{pid}(z) \in \mathbb{R}^3$ defined as

$$u_j^{pid}(z) := (u_{j,x}^{pd}(z), u_{j,y}^{pd}(z), u_{j,z}^{pid}(z)), \tag{12}$$

where

$$\begin{aligned} u_{j,x}^{pd}(z) &:= -m_j (k_{p,x}^j e_1^T (p_j - p_j^\star) + k_{d,x}^j e_1^T v_j) \\ u_{j,y}^{pd}(z) &:= -m_j (k_{p,y}^j e_2^T (p_j - p_j^\star) + k_{d,y}^j e_2^T v_j) - \cdots \\ &\quad \cdots - m_j d_j l_j \left(k_{p,\psi}^j e_2^T n + k_{d,\psi}^j e_3^T \omega \right) \\ u_{j,z}^{pid}(z) &:= -m_j (k_{p,z}^j e_3^T (p_j - p_j^\star) + k_{d,z}^j e_3^T v_j + k_{i,z}^j \xi_j) \end{aligned}$$

where $p_1^\star, p_2^\star$ are the UAVs equilibrium positions given in (9); where, for $l \in \{x, y, \mathrm{z}, \psi\}$, $k_{p,l}^j$ and $k_{d,l}^j$ are positive gains related to the position and velocity feedback, respectively, of vehicle $j \in \{1,2\}$ and the bar's yaw attitude; and where $k_{i,z}^j$ is a positive gain related to the integral feedback of vehicle $j \in \{1,2\}$.

Remark 2: The real control law is subject to saturations [24], which are of practical importance. Since these saturations do not interfere with the analysis we perform in the next sections, we omit them here for brevity.

Let us provide some insight into the control law (12) (and recall that we wish to align the bar with the inertial x direction, i.e., $n^\star = e_1$). The control law along the x-direction ($u_{j,x}^{pd}$) is composed of two terms, one proportional and one derivative that try to bring the UAV to its desired x position: this control law will only influence the x linear motion of the bar, and the x linear motion between the UAVs. The control law along the y-direction ($u_{j,y}^{pd}$) is composed of four terms: one proportional and one derivative that try to bring the UAV to its desired y position; and one proportional and one derivative that try to bring the bar to its desired y angular position: this control law will only influence the y linear motion of the bar, as well as the y angular motion of the bar (the yaw motion). Finally, the control law along the z-direction ($u_{j,z}^{pid}$) is composed of three terms: a proportional, a derivative and an integral that try to bring the UAV to its desired z position: this control law will only influence the z linear motion of the bar, as well as the z angular motion of the bar (the pitch motion). Given the equilibrium input defined in (10), the complete control law is then defined as

$$\mathbb{Z} \ni z \mapsto u^{cl}(z) := u^\star|_{m=\hat{m}} + (u_1^{pid}(z), u_2^{pid}(z)) \in \mathbb{R}^6,$$

where $\hat{m}$ is the mass of the bar as known by the controller: e.g., if the the bar's weight is known, then $\hat{m} := m$, and if the bar's weight is unknown, then $\hat{m} := 0$. It then follows that for (see Problem 1 and (10))

$$(\xi_1^\star, \xi_2^\star) := \left(\frac{g}{k_{i,z}^1} \frac{(m-\hat{m}) d_2}{m_1 (d_2 - d_1)}, \frac{g}{k_{i,z}^2} \frac{(m-\hat{m}) d_1}{m_2 (d_1 - d_2)} \right) \Rightarrow u^{cl}(z^\star) = u^\star, \tag{13}$$

where we emphasize that if the bar's mass is known, then the equilibrium integral errors vanish, i.e., $(\xi_1^\star, \xi_2^\star) = (0,0)$; however, even if the bar's weight is known, having an integral action is still of practical importance as it provides robustness against other types of model uncertainties. In the next sections, we study the stability of the equilibrium $z^\star$ (with $(\xi_1^\star, \xi_2^\star)$ as in (13)) of the closed loop vector field

$$z \mapsto Z^{cl}(z) := Z(z, u^{cl}(z)). \tag{14}$$

V. Routh's Criterion

In Section VI, we linearize the closed loop vector field Z^{cl} in (14) around the equilibrium $z^\star$ in (9), and we verify that the Jacobian is similar to a block triangular matrix, whose block diagonal entries are in controllable form. This section provides tools for the analysis of the eigenvalues of those matrices in controllable form. Denote then, for any $n \in \mathbb{N}$, and given an $a \in \mathbb{R}^n$, $C_n(a) := \begin{bmatrix} e_2 & \cdots & e_n & -a \end{bmatrix}^T \in \mathbb{R}^{n\times n}$, as a matrix in controllable form. It follows from the Routh's criterion that

$$C_3((a_0, a_1, a_2)) \text{ is Hurwitz} \Leftrightarrow a_0, a_1, a_2 > 0 \wedge a_0 < a_1 a_2, \tag{15}$$

which we make use of later on. In what follows, denote $q \in \mathbb{R}$, $f := (f_p, f_d) \in (\mathbb{R}_{\geq 0})^2$, $k := (k_p, k_d) \in (\mathbb{R}_{\geq 0})^2$, where, in later sections, q and f provide physical constants of interest, and k provides the controller gains (in particular a proportional and a derivative gain). There are two matrices (in controllable form) that appear several times in Section VI, and therefore we introduce them here. Specifically, we define Γ_3 and Γ_5 as

$$\Gamma_3(f, k) := C_3((f_d(k_p + f_p), f_d k_d + f_p, f_d)), \tag{16}$$

$$\Gamma_5(q, f, k) := C_5(e), \tag{17}$$

$$e \equiv f_d \left(k_p, f_p k_d, k_p + f_p(1+q), k_d + \tfrac{f_p}{f_d}(1+q), 1 \right).$$

Since we are interested in determining the stability of an equilibrium, it proves useful to determine when a matrix is Hurwitz. That it is the case iff all the elements in the first column of the Routh's table are positive (or negative) [25]. It follows from the Routh's criterion that (16) and (17) are Hurwitz if and only if

$$q > 0 \text{ and } f_d > k_p / k_d. \tag{18}$$

VI. Linearization

Before linearizing the closed loop vector field Z^{cl} in (14) around the equilibrium $z^\star$ in (9), let us provide a vector field that serves only the purpose of analysis. Recall the map f in (3) containing the constraints that define the state space. Consider then, for any $z \in \mathbb{R}^{32}$ and for some $\lambda > 0$,

$$\tilde{Z}(z) = -f'(z^\star)^T \left(f'(z^\star) f'(z^\star)^T\right)^{-1} \left(f'(z) Z^{cl}(z) + \lambda f(z)\right), \tag{19}$$

where, it follows from (2) and (8), that for any $z \in \mathbb{Z}$, $\tilde{Z}(z) = 0_{32}$. Consider then the new vector field

$$\bar{Z}^{cl}(z) := Z^{cl}(z) + \tilde{Z}(z), \tag{20}$$

where we emphasize that $\bar{Z}^{cl}(z) = Z^{cl}(z)$ for any $z \in \mathbb{Z}$. The sole purpose of the vector field $\tilde{Z}$ in (19) is to permit the analysis we conduct next.

Linearization of the closed loop vector field $\bar{Z}^{cl}$ in (20) around $z^\star$ in (9) yields the Jacobian

$$A := D\bar{Z}(z^\star) \in \mathbb{R}^{32\times 32}, \tag{21}$$

which is not a diagonal matrix, and thus determining whether it is Hurwitz is not straightforward. For that purpose, we provide a similarity matrix, i.e., $P \in \mathbb{R}^{32\times 32}$, such that PAP^{-1} is a block triangular matrix, and where each block diagonal matrix is in controllable form (allowing us to invoke the results from Section V). Consider then

$$P := \begin{bmatrix} P_{\mathrm{z}} & P_\theta & P_x & P_\delta & P_y & P_\psi & P_\perp \end{bmatrix}^T \in \mathbb{R}^{32\times 32}, \tag{22}$$

where (below A is the Jacobian in (21), and $e_1, \cdots, e_{32}$ are the canonical basis vectors in $\mathbb{R}^{32}$)

$$P_{\mathrm{z}} := \begin{bmatrix} \nu & A\nu & A^2\nu \end{bmatrix}\big|_{\nu = \frac{d_2 e_{31} - d_1 e_{32}}{d_2 - d_1}} \in \mathbb{R}^{32\times 3},$$

$$P_\theta := \begin{bmatrix} \nu & A\nu & A^2\nu \end{bmatrix}\big|_{\nu = \frac{e_{31} - e_{32}}{d_2 - d_1}} \in \mathbb{R}^{32\times 3},$$

$$P_x := \begin{bmatrix} e_1 & Ae_1 & A^2 e_1 & A^3 e_1 & A^4 e_1 \end{bmatrix} \in \mathbb{R}^{32\times 5},$$

$$P_\delta := \begin{bmatrix} \nu & A\nu & A^2\nu \end{bmatrix}\big|_{\nu = e_7 - e_{10}} \in \mathbb{R}^{32\times 3},$$

$$P_y := \begin{bmatrix} e_2 & Ae_2 & A^2 e_2 & A^3 e_2 & A^4 e_2 \end{bmatrix} \in \mathbb{R}^{32\times 5},$$

$$P_\psi := \begin{bmatrix} e_5 & Ae_5 & A^2 e_5 & A^3 e_5 & A^4 e_5 \end{bmatrix} \in \mathbb{R}^{32\times 5},$$

and, finally, where $P_\perp := (f'(z^\star))^T \in \mathbb{R}^{32\times 8}$.

Remark 3: Recall the state decomposition in (1), and that $\dot{z} = Az$, for the linearized motion around the equilibrium. Then (for brevity, denote $p = (x, y, \mathrm{z})$ and $n = (\cdot, \psi, \theta)$)

$$\begin{bmatrix} P_x^T z \\ P_\delta^T z \\ P_y^T z \\ P_\psi^T z \end{bmatrix} = \begin{bmatrix} (x^{(0)}, x^{(1)}, x^{(2)}, x^{(3)}, x^{(4)}) \\ (\delta^{(0)}, \delta^{(1)}, \delta^{(2)})|_{\delta = e_1^T(p_1 - p_2)} \\ (y^{(0)}, y^{(1)}, y^{(2)}, y^{(3)}, y^{(4)}) \\ (\psi^{(0)}, \psi^{(1)}, \psi^{(2)}, \psi^{(3)}, \psi^{(4)}) \end{bmatrix},$$

and (the equalities below can only be verified under an appropriate coordinate transformation)

$$\begin{bmatrix} P_{\mathrm{z}}^T z \\ P_\theta^T z \end{bmatrix} = \begin{bmatrix} (\mathrm{z}^{(-1)}, \mathrm{z}^{(0)}, \mathrm{z}^{(1)}) \\ (\theta^{(-1)}, \theta^{(0)}, \theta^{(1)}) \end{bmatrix}.$$

That is, P_x is associated with the x-linear motion of the bar (fifth order system) and P_δ is associated with the x-linear motion between the UAVs (third order system); P_y is associated with the y-linear motion of the bar (fifth order system) and P_ψ is associated with the y-angular motion of bar (fifth order system). And finally, P_{z} is associated with the z-linear motion of the bar (third order system) and P_θ is associated with the z-angular motion of bar (third order system). (The sum of the integral errors is then associated with the z-linear position of the bar, and the difference is associated with the z-angular position of the bar.)

Given the state matrix A in (21) and the similarity matrix P in (22), it then follows that

$$PAP^{-1} = \begin{bmatrix} A_{\mathrm{z},\theta} \oplus A_{x,\delta} \oplus A_{y,\psi} & \star \\ 0_{8\times 24} & -\lambda I_{8\times 8} \end{bmatrix} \in \mathbb{R}^{32\times 32}, \tag{23}$$

where (23) is a block triangular matrix, with the first block as a block diagonal matrix with three blocks (note that the λ in (23) is that chosen in (19)). Thus $\mathrm{eig}(A) = \{-\lambda\} \cup \mathrm{eig}(A_{\mathrm{z},\theta}) \cup \mathrm{eig}(A_{x,\delta}) \cup \mathrm{eig}(A_{y,\psi})$, and, therefore, determining whether the Jacobian A in (21) is Hurwitz amounts to checking whether each of the three blocks in (23) is Hurwitz. Let us look at each of these matrices separately, corresponding to three decoupled motions: longitudinal, lateral and vertical.

A. Longitudinal motion

Recall Remark 3, and note that P_x and P_δ are associated to $A_{x,\delta} \in \mathbb{R}^{8\times 8}$ in (23). As such, $A_{x,\delta}$ is associated with the longitudinal motion, namely the x motion of the bar, and the x motion difference between the two UAVs.

In what follows denote

$$F_x \equiv F_x(k_{p,x}^1, k_{p,x}^2, k_{d,x}^1, k_{d,x}^2, k_r^1, k_r^2) \in \mathbb{R}^3,$$

where F_x is some function of the gains shown above. Note then that $A_{x,\delta}$ has a specific structure, namely (below $\star$ denotes a vector in $\mathbb{R}^5$)

$$A_{x,\delta} = \begin{bmatrix} A_x & e_5 F_x^T \\ e_3 \star^T & A_\delta \end{bmatrix} \in \mathbb{R}^{(5+3)\times(5+3)}. \tag{24}$$

Notice that $A_{x,\delta}$ can be rendered block triangular, if one chooses the gains such that F_x in (24) vanishes. That is accomplished if, for $i \in \{1, 2\}$,

$$\begin{aligned} k_{p,x}^i &= k_{p,x} + \frac{d_i l_i}{d_1 l_1 - d_2 l_2} f_p \Delta_x, \\ k_{d,x}^i &= k_{d,x} + \frac{d_i l_i}{d_1 l_1 - d_2 l_2} \frac{f_p}{k_r} \Delta_x, \\ k_r^1 &= k_r^2 = k_r, \text{ and } \Delta_x = \frac{m(d_1 l_1 m_1 + d_2 l_2 m_2)}{m_1 m_2 (d_1 l_1 - d_2 l_2)}, \end{aligned} \tag{25}$$

for some positive $k_{p,x}$, $k_{d,x}$, and k_r, and where f_p is that in (27). That is, the proportional and derivative gains of each vehicle must be the same up to some difference that is proportional to the asymmetry of the system – quantized by Δ_x. If the vehicles' gains are chosen as above, then

$$A_{x,\delta} = \begin{bmatrix} A_x & 0_{5\times 3} \\ \star_{3\times 5} & A_\delta \end{bmatrix} \in \mathbb{R}^{8\times 8} \tag{26}$$

where (recall Γ_5 in (17))

$$\begin{aligned} A_x &= \Gamma_5\left(q, f, k\right)|_{f_d = k_r, k = (k_{p,x}, k_{d,x})}, \\ f_p &= \frac{g(l_1 + l_2)}{2 l_1 l_2} > 0, q = \frac{m(d_1^2 l_1^2 m_1 + d_2^2 l_2^2 m_2)}{m_1 m_2 (d_1 l_1 + d_2 l_2)^2} > 0, \end{aligned} \tag{27}$$

and where (recall Γ_3 in (16))

$$A_\delta = \Gamma_3\left(f, k\right)|_{\substack{f_d = k_r, k = (k_{p,x}, k_{d,x}), \\ f_p = \frac{g m (d_1^2 l_1^2 m_1 + d_2^2 l_2^2 m_2)}{l_1 l_2 m_1 m_2 (d_1^2 l_1 - d_1 d_2 (l_1 + l_2) + d_2^2 l_2)}}}.$$

It follows from (18) that A_x and A_δ above are Hurwitz, provided that

$$k_r > k_{p,x}/k_{d,x}.$$

provided that the attitude gain is big enough. This constraint can be comprehended intuitively: fast tracking along the longitudinal direction requires a fast attitude inner loop.

Remark 4: If the system is symmetric (see (24)), then

$$A_x = \Gamma_5\left(q, f, k\right)|_{q = \frac{m}{2M}, (f_p, f_d) = (\frac{g}{l}, k_r), k = (k_{p,x}, k_{d,x})}.$$

That is, the (linearized) x motion of the bar is exactly that of container in a container-crane system, with a cable of length l, being pulled by a crane of mass $2M$, and with a motor constant k_r [24].

Remark 5: If one wishes both gains $k_{p,x}^1$ and $k_{p,x}^1$, in (25), to be positive, then one must impose that $k_{p,x} >$

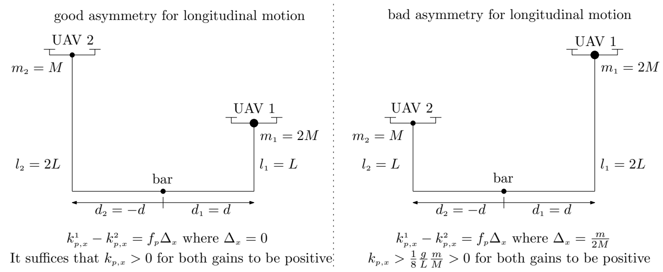

Fig. 3: Good and bad asymmetries (a good asymmetry only requires the gains $k_{p,x}, k_{d,x}$ to be positive, and a bad asymmetry requires the proportional gain to be strictly positive): it is better for the heavier UAV to be attached to the shorter cable.

$-f_p \frac{\min(d_1 l_1 \Delta_x, d_2 l_2 \Delta_x)}{d_1 l_1 - d_2 l_2}$, where Δ_x encapsulates some measure of asymmetry of the system. As illustrated in Fig. 3, there are *good and bad* asymmetries: in *good* asymmetries $\Delta_x = 0$ and, therefore, it is only required that $k_{p,x}$ be positive; and, in *bad* asymmetries $\Delta_x \neq 0$ and, therefore, it is required that $k_{p,x}$ be strictly positive.

Remark 6: Recall Remark 3. It follows from (26) that, for the linearized motion, (denote $X := (x^{(0)}, \cdots, x^{(4)})$ and $\Delta := (\delta^{(0)}, \cdots, \delta^{(2)})$)

$$\begin{bmatrix} \dot{X} \\ \dot{\Delta} \end{bmatrix} = \begin{bmatrix} A_x & 0_{5\times 3} \\ \star_{3\times 5} & A_\delta \end{bmatrix} \begin{bmatrix} X \\ \Delta \end{bmatrix},$$

i.e., the x motion behaves as a fifth order integrator and decoupled from the δ motion; while the δ motion behaves as a third order integrator, cascaded after the x motion.

B. Lateral motion

Recall Remark 3, and note that P_y and P_ψ are associated to $A_{y,\psi} \in \mathbb{R}^{10\times 10}$ in (23). As such, $A_{y,\psi}$ is associated with the lateral motion, namely the y linear motion of the bar, and the y angular motion of the bar (yaw motion). In what follows denote

$$F_y \equiv F_y(k_{p,y}^1, k_{p,y}^2, k_{d,y}^1, k_{d,y}^2, k_{p,\psi}^1, k_{p,\psi}^2, k_{d,\psi}^1, k_{d,\psi}^2, k_r^1, k_r^2) \in \mathbb{R}^5,$$

where F_y is some function of the gains shown above. Note then that $A_{y,\psi}$ has a specific structure, namely

$$A_{y,\psi} = \begin{bmatrix} A_y & e_5 F_y^T \\ e_5 \tilde{F}_y^T & A_\psi \end{bmatrix} \in \mathbb{R}^{(5+5)\times(5+5)}. \tag{28}$$

Notice that $A_{y,\psi}$ can be rendered block triangular, if one chooses the gains such that F_y in (28) vanishes (no choice of gains makes $\tilde{F}_y$ vanish). Similarly to as in Subsection VI-A, F_y vanishes under an appropriate choice of gains, which we omit here for brevity (details are found [24]). We only state here that

$$\begin{aligned} A_y &= \Gamma_5\left(q, f, k\right)|_{q = \bar{q}, f_p = \bar{f}_p, f_d = k_r, k = (k_{p,y}, k_{d,y})}, \\ A_\psi &= \Gamma_5\left(q, f, k\right)|_{q = \tilde{q}, f_p = \tilde{f}_p, f_d = k_r, k = (k_{p,y}, k_{d,y})}, \end{aligned}$$

for some positive $\bar{q}, \tilde{q}, \bar{f}_p, \tilde{f}_p$; and which are both Hurwitz, provided that

$$k_r > k_{p,y}/k_{d,y},$$

i.e., provided that the attitude gain is big enough. Note that similar remarks to Remarks 4, 5 and 6 can be made at this point regarding the lateral motion.

C. Vertical motion

Remark 7: In this section, and for brevity, we assume $d_1 = -d_2 =: d$ (for some d) when presenting the results. The results without these assumptions are found in [24]. Recall Remark 3, and note that P_z and P_θ are associated to $A_{z,\theta} \in \mathbb{R}^{6\times 6}$ in (23). As such, $A_{z,\theta}$ is associated with the vertical motion, namely the z linear motion of the bar, and the z angular motion of the bar (pitch motion).

In what follows denote

$$F_z \equiv F_z(k^1_{p,z}, k^2_{p,z}, k^1_{d,z}, k^2_{d,z}, k^1_{i,z}, k^2_{i,z},) \in \mathbb{R}^3,$$

where F_z is some function of the gains shown above. Note then that $A_{z,\theta}$ has a specific structure, namely

$$A_{z,\theta} = \begin{bmatrix} A_z & e_3 F_z^T \\ e_3 \tilde{F}_z^T & A_\theta \end{bmatrix} \in \mathbb{R}^{(3+3)\times(3+3)}. \quad (29)$$

Notice that $A_{z,\theta}$ can be rendered block triangular, if one chooses the gains such that either F_z or $\tilde{F}_z$ in (29) vanish. We choose to cancel F_z, implying that we decouple the z-linear motion, from the z-angular motion. That is accomplished if ($i \in \{1, 2\}$)

$$\frac{k^1_{p,z}}{k^2_{p,z}} = \frac{k^1_{d,z}}{k^2_{d,z}} = \frac{k^1_{i,z}}{k^2_{i,z}} = \frac{m_2(J + 2d^2 m_1)}{m_1(J + 2d^2 m_2)}.$$

That is, the proportional, derivative and integral gains of each vehicle must respect a ratio, which is exactly 1 under symmetry conditions (see (11)). In order to satisfy the conditions above, let, for $h \in \{p, i, d\}$,

$$\begin{aligned} k^1_{h,z} &= \frac{2(J + 2d^2 m_1)m_2}{4d^2 m_1 m_2 + J(m_1 + m_2)} k_{h,z}, \\ k^2_{h,z} &= \frac{2(J + 2d^2 m_2)m_1}{4d^2 m_1 m_2 + J(m_1 + m_2)} k_{h,z}, \end{aligned} \quad (30)$$

for some positive $k_{p,z}$, $k_{d,z}$, and $k_{i,z}$. If the vehicles' gains are chosen as in (30), then

$$A_{z,\theta} = \begin{bmatrix} A_z & 0_{3\times3} \\ \star_{3\times3} & A_\theta \end{bmatrix} \in \mathbb{R}^{(3+3)\times(3+3)}$$

where (recall C_3 in (15))

$$\begin{aligned} A_z &= C_3 \left(\gamma_z(k_{p,z}, k_{d,z}, k_{i,z})\right), \\ A_\theta &= C_3 \left(\gamma_\theta(k_{p,z}, k_{d,z}, k_{i,z})\right), \end{aligned}$$

and where

$$\gamma_z = \frac{4m_1 m_2 (J+2d^2 m_1)(J+2d^2 m_2)}{(4d^2 m_1 m_2 + J(m_1+m_2))(J(m+m_1+m_2)+d^2(4m_1 m_2 + (m_1+m_2)m))},$$

$$\gamma_\theta = \frac{4d^2 m_1 m_2}{4d^2 m_1 m_2 + J(m_1+m_2)}.$$

It follows from (15) that A_z and A_θ are Hurwitz (and therefore also $A_{z,\theta}$), provided that

$$k_{i,z} < \min(\gamma_z, \gamma_\theta) k_{p,z} k_{d,z}.$$

i.e., provided that the integral gain is *small enough*. Note that, for a regular PID, it is required that $k_{i,z} < k_{p,z} k_{d,z}$, while the constraint above is more restrictive, since $\gamma_\theta < 1$. Moreover, notice that γ_θ vanishes when d vanishes (the distance of the contact points to the bar's center of mass): as such, it is advisable to have a *big* d (*big* compared with $\sqrt{\frac{J(m_1+m_2)}{m_1 m_2}}$), because γ_θ is closer to 1 (and thus the bound on the integral gain is less restrictive). This also agrees with intuition, which suggests that controlling the bar's attitude when the contact points are too close to the bar's center of mass is difficult.

Remark 8: The attitude gains of the vehicles do not play a role in the linearized vertical motion.

VII. Experimental Results

A video of the experiment that is described in the sequel is found at https://youtu.be/rgweowQ8fAE, whose results are visualized in Fig. 4. For the experiment, two hexacopters were used, namely one ASTEC-Neo weighting 2.22 kg, and one Tarot FY680 weighting 3.53 kg. The bar was made out of a core of aluminum, surrounded with PVC pipe, and with two metal plates at the contact points with the cables: in total, it weighted 1.48 kg, with the individual plates weighting 0.6 kg each (the bar's weight corresponds to 60% of the ASTEC-Neo and to 40% of the Tarot FY680). The bar has a length of 2m, with the contact points between the bar and the cables at the extremities of the bar, and thus $d_1 = -d_2 = 1$ m; the cables are attached to the bar's contact points by means of permanent magnets. The ASTEC-Neo is tethered to the bar by a 1.45 m cable, and the Tarot FY680 by a 1.2 m cable. The commands for controlling the hexacopter were processed on a ground station, developed in a ROS environment, and sent to the on-board autopilot, which allowed for remotely controlling the aerial vehicles. The ASTEC-Neo is equipped with a proprietary flight controller, which we communicate with by publishing a message of the type mav_msgs/RollPitchYawrateThrust; while the Tarot FY680 is equipped with an open source flight controller (namely a PixHawk), which we communicate with by publishing a message of the type mavros_msgs/OverrideRCIn. The hexacopter's and the bar's poses and twists were estimated by 12 cameras from a Qualisys motion capture system.

In the beginning of the experiment the bar is required to stabilize around $z^\star$ (see (9)) where $p^\star = (0.4, -0.5, 0.4)$m and $n^\star = e_2$ (see Remark 1), i.e, the bar is required to hover at 0.4m and required to be aligned with the y-axis. In Fig. 4(b), the bar attitude is parameterized with a pitch and yaw angle (i.e., $n = (\cos(\theta)\cos(\psi), \cos(\theta), \sin(\theta))$), and, as can be seen in Fig. 4(b) the bar is initially aligned with the y-axis ($\psi = 90°$). At around 55 sec, the bar is required to translate 0.5m in the x-direction, and at around 60 sec, the bar is required to align itself with the x-axis ($n^\star = e_1 :\Leftrightarrow \psi^\star = 0°$), which can be seen in Figs. 4(a) and 4(a). At around 80 sec, the bar is required to move in the y-direction, while keeping the same orientation, which can again be seen in Figs. 4(a) and 4(a). During the same experiment, we also tested robustness against impulse disturbances, which illustrate the size of the basin of attraction of the equilibrium. First, at around 100s, we disturbed the Tarot FY680 in the y-direction, as can be seen in Fig. 4(d); and, at around 110s, we disturbed the ASTEC-Neo in the y-direction, as can be seen in Fig. 4(c). In both cases, the system returns to its

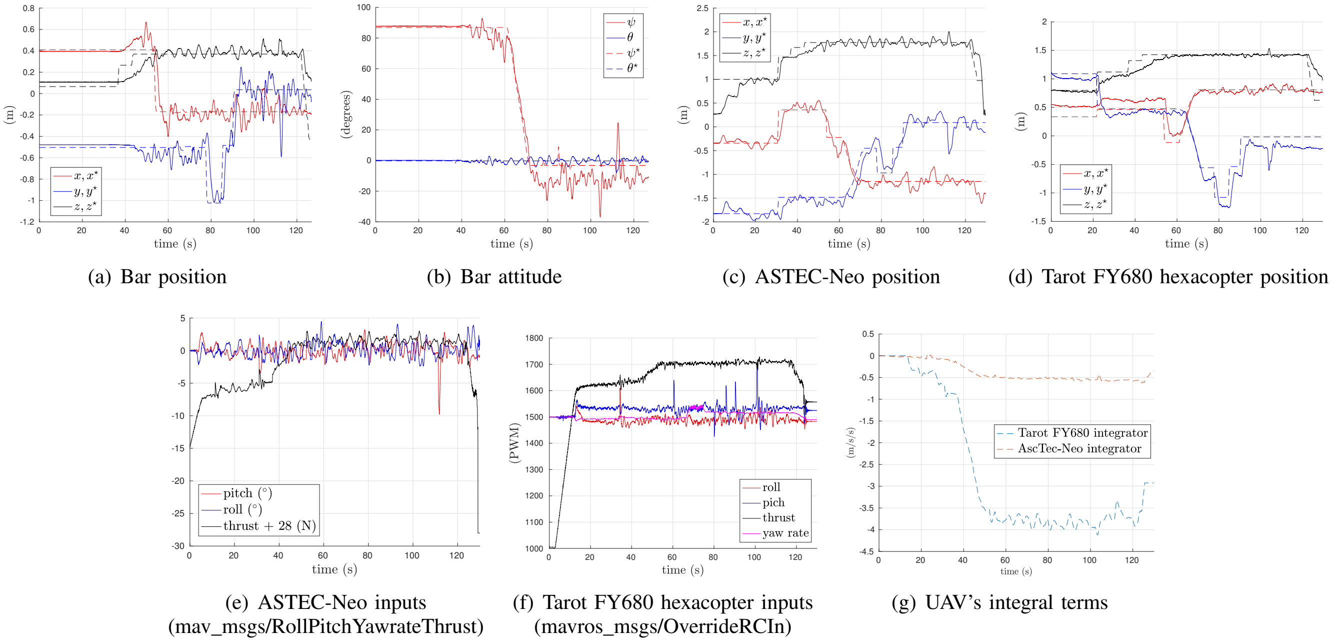

(a) Bar position (b) Bar attitude (c) ASTEC-Neo position (d) Tarot FY680 hexacopter position

(e) ASTEC-Neo inputs (mav_msgs/RollPitchYawrateThrust) (f) Tarot FY680 hexacopter inputs (mavros_msgs/OverrideRCIn) (g) UAV's integral terms

Fig. 4: Experimental results for collaborative bar transportation tethered to non-identical hexacopters.

equilibrium point.

In Figs. 4(e) and 4(f), the control inputs are shown, and in Fig. 4(g) the integral terms for both UAVs are shown. The equilibrium integral term is inversely proportional to the vehicle's weight, which explains why the integral term for the ASTEC-Neo is smaller than that for the Tarot FY680.

References

[1] AEROWORKS aim. http://www.aeroworks2020.eu/.

[2] S. J. Lee and H. J. Kim. Autonomous swing-angle estimation for stable slung-load flight of multi-rotor UAVs. In *IEEE International Conference on Robotics and Automation*, pages 4576–4581, May 2017.

[3] M. Bisgaard, A. la Cour-Harbo, and J. D. Bendtsen. Adaptive control system for autonomous helicopter slung load operations. *Control Engineering Practice*, 18(7):800 – 811, 2010. Special Issue on Aerial Robotics.

[4] I. Palunko, R. Fierro, and P. Cruz. Trajectory generation for swing-free maneuvers of a quadrotor with suspended payload: A dynamic programming approach. In *IEEE International Conference on Robotics and Automation*, pages 2691–2697, May 2012.

[5] S. Tang and V. Kumar. Mixed integer quadratic program trajectory generation for a quadrotor with a cable-suspended payload. In *IEEE International Conference on Robotics and Automation*, pages 2216–2222, May 2015.

[6] M. Tognon and A. Franchi. Dynamics, control, and estimation for aerial robots tethered by cables or bars. *IEEE Transactions on Robotics*, 33(4):834–845, Aug 2017.

[7] R. Mebarki, V. Lippiello, and B. Siciliano. Toward image-based visual servoing for cooperative aerial manipulation. In *IEEE International Conference on Robotics and Automation*, pages 6074–6080, May 2015.

[8] S. Kim, S. Choi, H. Lee, and H. J. Kim. Vision-based collaborative lifting using quadrotor UAVs. In *2014 14th ICCAS*, pages 1169–1174, Oct 2014.

[9] M. Gassner, T. Cieslewski, and D. Scaramuzza. Dynamic collaboration without communication: Vision-based cable-suspended load transport with two quadrotors. In *IEEE International Conference on Robotics and Automation*, pages 5196–5202, May 2017.

[10] H. Lee, H. Kim, and H. J. Kim. Planning and control for collision-free cooperative aerial transportation. *IEEE Transactions on Automation Science and Engineering*, PP(99):1–13, 2017.

[11] H. Kim, H. Lee, S. Choi, Y. k. Noh, and H. J. Kim. Motion planning with movement primitives for cooperative aerial transportation in obstacle environment. In *IEEE International Conference on Robotics and Automation*, pages 2328–2334, May 2017.

[12] H. Lee, H. Kim, and H. J. Kim. Path planning and control of multiple aerial manipulators for a cooperative transportation. In *IEEE/RSJ IROS*, pages 2386–2391, Sept 2015.

[13] Q. Jiang and V. Kumar. The inverse kinematics of cooperative transport with multiple aerial robots. *IEEE Transactions on Robotics*, 29(1):136–145, Feb 2013.

[14] N. Michael, J. Fink, and V. Kumar. Cooperative manipulation and transportation with aerial robots. *Autonomous Robots*, 30(1):73–86, 2011.

[15] M. Mohammadi, A. Franchi, D. Barcelli, and D. Prattichizzo. Cooperative aerial tele-manipulation with haptic feedback. In *2016 IEEE/RSJ International Conference on Intelligent Robots and Systems*, pages 5092–5098, Oct 2016.

[16] C. Masone, H. H. Bülthoff, and P. Stegagno. Cooperative transportation of a payload using quadrotors: A reconfigurable cable-driven parallel robot. In *2016 IEEE/RSJ International Conference on Intelligent Robots and Systems*, pages 1623–1630, Oct 2016.

[17] D. Mellinger, M. Shomin, and V. Kumar. Control of quadrotors for robust perching and landing. In *Proceedings of the International Powered Lift Conference*, pages 205–225, 2010.

[18] A. Gawel, M. Kamel, T. Novkovic, J. Widauer, D. Schindler, B. P. von Altishofen, R. Siegwart, and J. Nieto. Aerial picking and delivery of magnetic objects with MAVs. In *IEEE International Conference on Robotics and Automation*, pages 5746–5752, May 2017.

[19] A. Tagliabue, M. Kamel, S. Verling, R. Siegwart, and J. Nieto. Collaborative transportation using MAVs via passive force control. In *IEEE International Conference on Robotics and Automation*, pages 5766–5773, May 2017.

[20] P. Pereira and D. V. Dimarogonas. Collaborative transportation of a bar by two aerial vehicles with attitude inner loop and experimental validation. In *IEEE Conference on Decision and Control*, pages 1815–1820, 2017.

[21] P. E. I. Pounds, D. R. Bersak, and A. M. Dollar. Grasping from the air: Hovering capture and load stability. In *IEEE International Conference on Robotics and Automation*, pages 2491–2498, May 2011.

[22] P. O. Pereira and D. V. Dimarogonas. Stability of load lifting by a quadrotor under attitude control delay. In *IEEE International Conference on Robotics and Automation*, pages 3287–3292, May 2017.

[23] M. Orsag, C. Korpela, M. Pekala, and P. Oh. Stability control in aerial manipulation. In *2013 American Control Conference*, pages 5581–5586, June 2013.

[24] P. Pereira, P. Roque, and D. V. Dimarogonas. Mathematica files used in obtaining the manuscript's results. In *https://github.com/KTH-SML/pose-stabilization-of-bar-tethered-to-two-uavs.git*.

[25] R. C. Nelson. *Flight Stability and Automatic Control*, volume 2. WCB/McGraw Hill, 1998.